


## Valley engineering electron-hole liquids in transition metal dichalcogenide monolayers

Arnab Barman Ray <sup>1</sup>, Kevin Liang,<sup>2</sup> and Anthony Nicholas Vamivakas<sup>1,\*</sup>

<sup>1</sup>*The Institute of Optics, University of Rochester, Rochester, New York 14627, USA*

<sup>2</sup>*Physics Department, Adelphi University, Garden City, New York 11530, USA*



(Received 8 May 2022; revised 29 June 2022; accepted 30 June 2022; published 22 July 2022)

Electron-hole liquids (EHLs), a correlated state of matter and a thermodynamic liquid, have recently been found to exist at room temperature in suspended monolayers of MoS<sub>2</sub>. Appreciably higher rates of radiative recombination inside the liquid as compared to free excitons hold promise for optoelectronic applications such as broadband lasing. In this paper, we show that leveraging the valley physics in MoS<sub>2</sub> may be a route towards achieving tunability of specific characteristics of an EHL, such as emission wavelength, linewidth, and, most importantly, the liquid density. The conditions under which EHLs form, in bulk semiconductors as well as transition metal dichalcogenide (TMDC) monolayers are quite stringent, requiring high crystal purity and cryogenic temperatures in bulk semiconductors, and suspension in monolayers. Using a simple yet powerful model for describing free excitons and show that a phase transition into the EHL state may be feasible in substrate-supported monolayer samples. More repeatable experimental realizations of EHLs may be essential to answer questions regarding the nature of electron-hole correlations and how they may be used to generate nontrivial states of light.

DOI: [10.1103/PhysRevB.106.045206](https://doi.org/10.1103/PhysRevB.106.045206)

### I. INTRODUCTION

The characteristic broad luminescence spectra associated with an electron-hole liquid (EHL) was first detected by Haynes at the Bell Telephone Laboratories in 1966, in a sample of silicon immersed in liquid helium, when the pump intensity exceeded a certain threshold [1]. Subsequent experiments in the late 1960s and early 1970s provided further evidence for EHLs. Keldysh first provided a theoretical foundation for a phase transition, a gas-liquid condensation in semiconductors at sufficiently low temperatures, where the interaction between electron and holes at large densities ( $10^{17} \text{ cm}^{-3}$ ) would cause them to condense from an insulating gas of free excitons and possibly multiexcitonic complexes into macroscopic metallic droplets of delocalized electrons and holes [2,3]. In Ge, experiments showing abrupt increases in photoconductivity [4] with laser pump intensity and collection of charge pulses in *p-n* junctions at high incident intensities [5] further established the distinctness of a metallic EHL from candidates like a dielectric  $H_2$ -like excitonic liquid or a Bose-Einstein condensate. Infrared scattering experiments showed the state existing as a fog of smaller droplets while large  $\mu\text{m}$ -sized droplets were found to form under certain conditions [6]. Theory and experiments agreed with each other, and, while open questions remained, the phenomenon faded into obscurity until recently when EHLs were realized at room temperatures in atomically thin semiconductors. Room temperature realization of these macroscopic quantum states has revived interest and relevance [7–11].

Using a suspended CVD-grown monolayer of MoS<sub>2</sub>, kept at room temperatures, a sharp transition in the photoluminescence spectrum was recently observed [8]. The A-exciton line disappears into a broad, redshifted peak at high power densities, accompanied by a corresponding reduction in the emission spot size. This transition was shown to be reversible, ruling out defect-generation as a cause for the observation. Theoretical calculations for EHL formation in two-dimensional TMDCs as well as thermodynamic analyses that use the latest standards for quantifying carrier interactions in TMDCs, with the use of the Keldysh potential, do show the possibility of such a transition for temperatures above 500 K [9,11]. Further evidence for the formation of an EHL has surfaced in graphene-encapsulated MoTe<sub>2</sub> in the form of abrupt changes in photocurrent across the monolayer at high laser intensities [10].

In experiments, the use of a suspended monolayer is crucial for two reasons. First, due to the reduced dielectric screening compared to substrate-supported samples, Coulomb interactions are stronger. Second, the lack of a constraining substrate allows the monolayer to undergo isotropic expansion, affecting a transition into an indirect band-gap semiconductor, imparting larger lifetimes to charge carriers and allowing them to reach a quasi-equilibrium state. This paper demonstrates the possibility of leveraging the unique spin-valley physics of TMDC monolayers to tune the EHL emission properties, the binding energy, emission linewidth, and liquid density. Using a simple model that captures the strength of electromagnetic interactions in monolayers, we show that, even with dielectric screening from a substrate, as long as the charge carriers stay in the system long enough, with lifetimes exceeding quasi-thermalization times [2], a phase transition into an EHL is theoretically feasible.

\*nick.vamivakas@rochester.edu

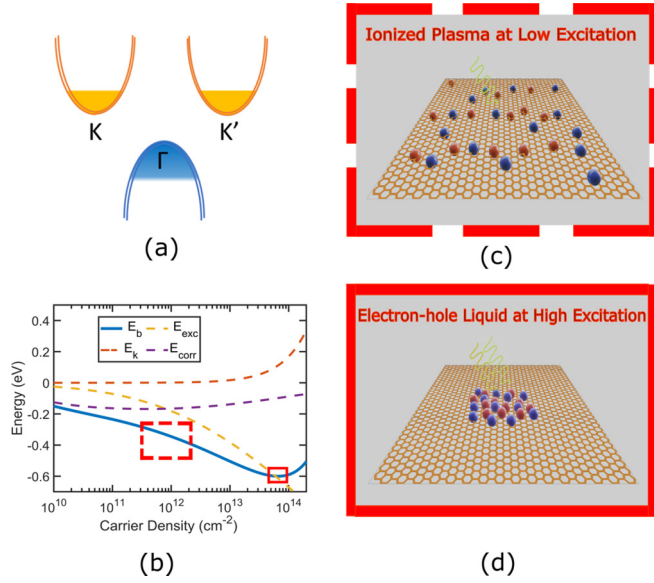


FIG. 1. (a) Band-energy diagram of monolayer MoS<sub>2</sub>, filled portions indicate the amount of charge carriers in a particular valley, (b) binding energy with carrier density—dashed and solid squares designate regions of ionized plasma vs EHL—as illustrated in (c) and (d) respectively.

## II. VALLEY ENGINEERING AN EHL

### A. Binding energy

The binding energy of an electron-hole pair in an EHL is found from the minima of the binding energy for a correlated plasma gas, consisting of electrons and holes, as the carrier density is varied. The binding energy of such a system consists of three parts,  $E_b = E_k + E_{\text{exc}} + E_{\text{corr}}$ , as a sum of the kinetic, exchange, and correlation energies. In keeping with the current understanding that an EHL arises out of an indirect band-gap transition for a monolayer of MoS<sub>2</sub>, the system consists of 2 nearly spin-degenerate electron bands at the  $K$  and  $K'$  points of the first Brillouin zone, and a spin-degenerate hole band at  $\Gamma$ , as shown in Fig. 1(a). It has been shown that the majority of holes reside at  $\Gamma$  at high carrier densities [12]. In the following, we calculate the binding energy in a manner similar to Rustagi *et al.* [9].

The first contribution to the energy per electron-hole ( $e$ - $h$ ) pair is the ground state, noninteracting kinetic energies of the electrons and holes. For the case of our model, we have

$$E_k = \frac{2\pi\hbar^2}{N_{eh}} \left( \int_0^{k_{eK}} dk \frac{k^3}{m_e} + \int_0^{k_{eK'}} dk \frac{k^3}{m_e} + \int_0^{k_{h\Gamma}} dk \frac{k^3}{m_h} \right), \quad (2.1)$$

where  $k_{eK}$ ,  $k_{eK'}$ , and  $k_{h\Gamma}$  are the Fermi wave vectors of the three valleys. For equal valley contributions,  $k_{eK} = k_{eK'} = \sqrt{\pi N_{eh}}$  and  $k_{h\Gamma} = \sqrt{2\pi N_{eh}}$ , where  $N_{eh}$  is the density of  $e$ - $h$  pairs.

The exchange energy that comes out of the requirement for antisymmetry in the many-body wave function is simply the expectation value of the interaction potential in the ground

state of the system and is given as:

$$E_{\text{exc}} = -\frac{1}{(2\pi)^2 N_{eh}} \left( \iint_{F_K} d\mathbf{k}\mathbf{k}' v(|\mathbf{k} - \mathbf{k}'|) + \iint_{F_{K'}} d\mathbf{k}\mathbf{k}' v(|\mathbf{k} - \mathbf{k}'|) + \iint_{F_\Gamma} d\mathbf{k}\mathbf{k}' v(|\mathbf{k} - \mathbf{k}'|) \right), \quad (2.2)$$

where  $v(|\mathbf{q}|) = \frac{1}{L^2} \frac{e^2}{2\epsilon_0(\epsilon_1 + \epsilon_2)|\mathbf{q}|(1+r|\mathbf{q}|)}$  with screening length [13]  $r = 4\pi r_0/(\epsilon_1 + \epsilon_2)$ , where  $r_0$  is the polarizability in TMDC monolayers [14]. The integrals are within the respective Fermi surfaces of the three valleys. Analytically, each of the three terms in Eq. (2) can be represented as  $E_{k_F} = E_1 + E_2$ , where  $E_1 = -\frac{4k_F^2}{3\pi N_{eh}}$ , and  $E_2 = -\frac{2\pi k_F^2}{N_{eh}} \int_{-\infty}^{\infty} \frac{r}{\pi^2 x^2} G_{3,1}^{1,3} \left[ 4 \left( \frac{r}{x} \right)^2 \middle| \begin{matrix} 0, 0 \\ \frac{1}{2} \end{matrix} \right] \left( \frac{J_1(k_F x)}{x} \right)^2 x dx$ , for a Fermi wave vector  $k_F$ . The  $G$  function here is the Meijer  $G$  function.

The correlation energy is the perturbative correction that arises from turning on the interaction between the fermions. It is related to the random-phase approximation (RPA) dielectric function,  $\epsilon_{RPA} = 1 - a_0(\mathbf{k}, \omega) - i\sigma_0(\mathbf{k}, \omega)$  through [15]

$$E_{\text{corr}} = -\frac{1}{4\pi N_{eh}} \int \frac{d\mathbf{k}}{(2\pi)^2} \int \hbar d\omega \times \left\{ \text{sgn}(\sigma) \frac{\sigma_0}{\sigma} \tan^{-1} \left( \frac{|\sigma|}{1-a} \right) - \sigma_0 \right\}. \quad (2.3)$$

For a single spin-degenerate band, the polarizabilities  $\sigma_l$  and  $a_l$  can be calculated as  $a_l + i\sigma_l = -2v(|\mathbf{k}|) \sum_q \frac{n_{k+q} - n_p}{\hbar\omega + E(\mathbf{q}) - E(\mathbf{q}+\mathbf{k})}$ , explicit values of which for isotropic 2D bands have been previously calculated [16]. The total polarizabilities  $\sigma_0$  and  $a_0$  are simply the sum of the respective terms for the 3 valleys. The exchange-corrected values of the polarizabilities, which arise out of the reduced correlation between electrons of the same spin due to Pauli exclusion are obtained as [17]:  $\sigma = (1 - h_{e1}(k))\sigma_0^{e1} + (1 - h_{e2}(k))\sigma_0^{e2} + (1 - h_h(k))\sigma_0^h$ , where  $h(k) = v(\sqrt{k^2 + f^2})/2v(k)$  is the correction term for a valley with Fermi wave vector  $f$ . The real part of the corrected polarizability  $a$  is given by,  $a = \frac{\sigma}{\sigma_0} a_0$ .

We chose values of the conduction band-effective mass from *ab initio* studies,  $m_e = 0.55$  [14,18], and the effective mass in the  $\Gamma$  Valley is taken to be  $m_h = 2.0$ , in order to obtain agreement with reported values of the linewidth, or the energy-edge width, as we show next. This value of the mass is consistent with a computational study of valley masses in strained and unstrained monolayers [19].

The binding energy is shown in Fig. 1(b) as a function of carrier density. The minima at around  $n_{eh} = 6.5 \times 10^{13} \text{ cm}^{-2}$  imparts the plasma with the properties of a thermodynamic liquid with a well-defined density and volume. We note that the liquid density calculated here is higher than previous reports [8], as we believe that experimentally-obtained values of EHL density are underestimates, as EHL droplets exist in equilibrium with surrounding plasma inside the emission spot. The binding energy is estimated to be  $E_b^{eh} = -0.61 \text{ eV}$ . The energy-edge width, i.e., the difference between the high and low energy tails of EHL emission, would be the total of the Fermi energies in the CB and VB given by  $\Delta_E = E_{Kf} +$

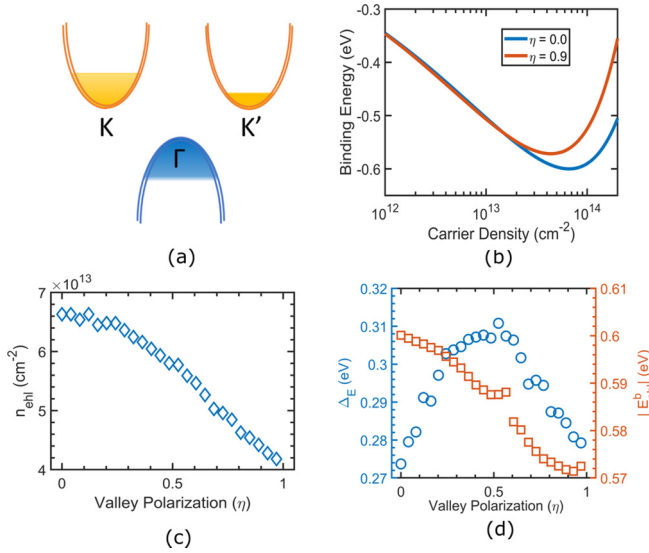


FIG. 2. (a) Band diagram illustrating valley polarization with unequal number of charge carriers in each valley, (b) binding energy diagrams for  $\eta = 0.0$  and  $\eta = 0.9$ , showing change with valley polarization, (c) EHL density with  $\eta$ , and (d) EHL binding energy and emission linewidth with  $\eta$ .

$E_{\Gamma f} + 2k_B T = 0.27$  eV, which is also consistent with the values observed experimentally (we use  $T = 460$  K). We note that these binding energies are orders of magnitude higher than those reported in bulk semiconductors at cryogenic temperatures owing to the strength of interactions in monolayers [20]. Such high binding energies allow the EHL to be observed experimentally at room temperatures. Figures 1(c) and 1(d) illustrate the qualitative features of charged species at a lower density and as an EHL respectively.

### B. Valley-induced EHL modulation

The selection rules in monolayer MoS<sub>2</sub> allow the charge carriers to have a net valley polarization depending on the polarization of the excitation laser. Using elliptical or circular polarization, one can induce a valley polarization in the population of charge carriers. This allows the possibility of establishing a knob on the average kinetic energy of the total carrier population. While both the exchange and correlation energies are affected, the kinetic energy is the most sensitive to valley polarizing carriers. We note that the optical transitions are direct and still across the valleys at  $K$  and  $K'$ , allowing a valley polarization, even though most holes reside at  $\Gamma$  after scattering at steady state.

Figure 2(a) illustrates the band diagram for a monolayer with valley polarization. In Fig. 2(b), we see that, while the EHL binding energy is mostly unaffected, the liquid density changes by an appreciable amount. The valley polarization is defined as

$$\eta = \frac{N_{ehK} - N_{ehK'}}{N_{ehK} + N_{ehK'}},$$

where  $N_{eh} = N_{ehK} + N_{ehK'}$  and the Fermi wave vectors for the two valleys are given as  $k_{eK} = \sqrt{2\pi \frac{1-\eta}{2} N_{eh}}$  and  $k_{eK'} =$

$\sqrt{2\pi \frac{1+\eta}{2} N_{eh}}$ . We note that, while a value of  $\eta = 0.9$  is unrealistic in monolayers even at cryogenic temperatures, there have been studies indicating 100% polarization in MoS<sub>2</sub> [21] with resonant excitation.

Figure 2(c) shows that  $n_{ehl}$  is tunable over a wide range of  $6.5 \times 10^{13}$  cm<sup>-2</sup> to  $4 \times 10^{13}$  cm<sup>-2</sup>. As the valley polarization is increased, the average kinetic energy of the system increases, causing the liquid to be more destabilized, and decreasing its density. While the linewidth of emission, now defined as  $\Delta E = \max(E_{Kf}, E_{K'f}) + E_{\Gamma f}$ , should increase continuously as the Fermi energy in one of the valleys keeps increasing, we find that due to the lowering liquid density, the two effects nearly compensate each other and the linewidth starts to decrease for  $\eta > 0.6$  as shown in Fig. 2(d). Hence, we can achieve around 10% increase in the emission linewidth. The change in binding energy is not appreciable within the studied range; however, due to band-gap renormalization effects at different carrier densities, one may expect the EHL emission to shift, or even become bimodal. This, however, is outside the scope of this work.

### III. FEASIBILITY OF AN EHL IN MGO-CAPPED SAMPLES

Suspended monolayers are hard to fabricate owing to their intrinsic fragility. Furthermore, there is the added complication of laser heating. At higher laser powers, of the order of a few kW/cm<sup>2</sup>, the monolayer experiences isotropic strain around  $\sim 1.25\%$  to become an indirect band-gap semiconductor, which is essential for the charge carriers to remain in the system long enough to reach a quasiequilibrium state. Recently, using thermally deposited oxide films, it has been demonstrated that high degrees of isotropic strain can be imparted to MoS<sub>2</sub> monolayers [22]. We investigate the dielectric feasibility of EHL formation in such kinds of samples, as illustrated in Fig. 3(b), with compressive thin films of MgO (IR dielectric constant, 2.6), where the monolayer is supported on an hBN layer.

We start with a simple Wannier-Mott model of 2D excitons in TMDC monolayers that allow us to accurately capture the effect of dielectric screening and carrier-carrier interactions (see Supplementary Material [23] for details). Figure 3(a) shows the ranges of calculated binding energies for different monolayer-substrate combinations and corresponding experimentally reported values [20,24–27]. Because the experimental values of carrier densities are inaccessible, we use a constant and experimentally accessible carrier density range of  $10^{11} - 10^{12}$  cm<sup>-2</sup>. We see that the model offers excellent qualitative agreement without the need for any fitting parameters. IR values of the dielectric constants are used in the calculation and are mentioned in the figure. Figure 3(c) demonstrates how the tunability of an EHL changes with increased environmental dielectric screening. We see that while the EHL density decreases with substrate screening, the degree of density modulation  $\sim 40\%$  remains mostly constant.

A transition from the excitonic response at low carrier densities is required for an EHL to form. While a complete thermodynamic analysis may be essential to ascertain whether a phase transition is feasible in the presence of environmental dielectric screening in substrate-supported samples, our

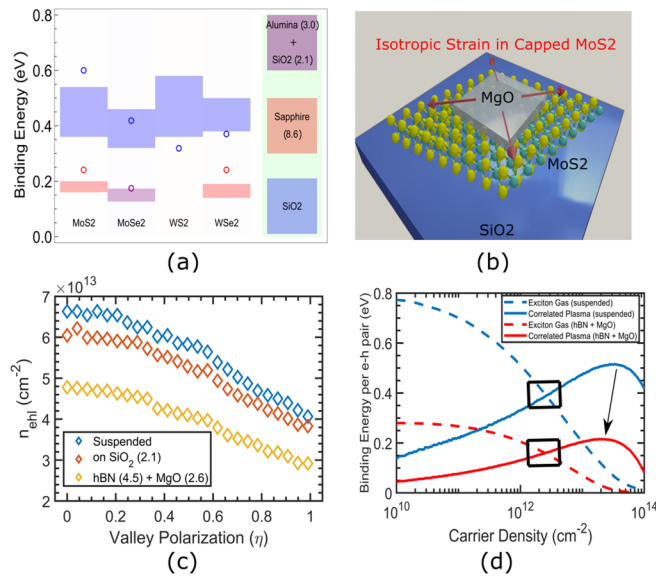


FIG. 3. (a) A comparison of calculated (shaded regions) and reported binding energies (open circles) for excitons, (b) schematics of capped monolayer MoS2 samples, (c) EHL density tuning for different substrate superstrate configuration (IR values of dielectric constants used are shown in the inset), and (d) exciton gas vs EHL competition for suspended and MgO-capped samples.

results for the EHL and excitonic gas can be combined to show that dielectric screening is not an impediment to the realization of an EHL state in MgO-capped samples, as shown in Fig. 3(d). The black arrow indicates the movement of the EHL state to lower densities. The black rectangles identify the regions of exciton-EHL crossover and illustrate no qualitative change in the nature of competition between these two states. We also note that the calculated binding energy of  $\sim 0.2$  eV for an EHL guarantees stability at room temperature.

#### IV. DISCUSSION AND CONCLUDING REMARKS

As we have shown here, valley engineering opens up the possibility of tuning the characteristics of EHL emission. The tunable liquid density may find applications in generating and detecting THz waves. Using a simple excitonic model,

we accurately capture the physics of dielectric screening and carrier interactions and apply it to assert the possibility of an EHL state forming in substrate-supported samples, even in the presence of dielectric screening. Hence, we conclude that as long as a monolayer strains into an indirect band gap, allowing charge carriers enough time to thermalize, an EHL state should be achievable.

We should note that EHLs in bulk semiconductors require high crystal purity. As such, the presence of defects and impurities in monolayers would hinder EHL formation by providing faster nonradiative decay channels for the charge carriers. Strain gradients in monolayers can serve as a way to funnel and move EHL droplets throughout the flake, as has been seen with bulk semiconductors. The effect of magnetic fields on the EHL emission is also an interesting direction for further studies [28,29].

High rates of radiative recombination inside a droplet ensure better photoluminescence quantum yield without the use of postprocessing techniques [30,31]. This holds promise for harnessing such collective phenomena for optoelectronic applications. Further broadening of the EHL emission may be achieved at higher temperatures at the expense of density tunability owing to lower liquid densities [9]. Moreover, other TMDC monolayers with different band gaps may be used as emission sources in other regions of the IR-visible spectrum. More accessible samples allowing highly repeatable realizations of EHLs are essential to answer some pertinent questions. The nature of the quantum mechanical electron-hole correlations present in the liquid—which, through quantum statistical state injection [32,33], may be transferred into the emitted photons—can allow perhaps, the creation of nontrivial quantum states of light. Delocalized holes and electrons across a droplet may give rise to spatially coherent emission. Also present are interesting questions about in-liquid mobility and resistance. Our results provide fresh and fertile ground for further experimental exploration.

#### ACKNOWLEDGMENTS

The authors thank Dr. Arunabh Mukherjee for discussions about the manuscript. This work was supported by AFOSR FA9550-19-1-0074 from the Cornell Center for Materials Research with funding from the NSF MRSEC program (DMR-1719875).

- [1] J. R. Haynes, *Phys. Rev. Lett.* **17**, 860 (1966).
- [2] L. V. Keldysh, *Contemp. Phys.* **27**, 395 (1986).
- [3] T. K. Lo, *Solid State Commun.* **15**, 1231 (1974).
- [4] V. M. Asnin and A. A. Rogachev, *JETP Lett.* **7**, 464 (1968).
- [5] V. M. Asnin, A. A. Rogachev, and N. L. Sablina, *JETP Lett.* **11**, 162 (1970).
- [6] C. D. Jeffries, *Science* **189**, 955 (1975).
- [7] S. Berciaud, *Nat. Photonics* **13**, 225 (2019).
- [8] Y. Yu, A. W. Bataller, R. Younts, Y. Yu, G. Li, A. A. Purotzky, D. B. Geohegan, K. Gundogdu, and L. Cao, *ACS Nano* **13**, 10351 (2019).
- [9] A. Rustagi and A. F. Kemper, *Nano Lett.* **18**, 455 (2018).
- [10] T. B. Arp, D. Pleskot, V. Aji, and N. M. Gabor, *Nat. Photonics* **13**, 245 (2019).
- [11] P. Pekh, P. Ratnikov, and A. Silin, *JETP Lett.* **111**, 90 (2020).
- [12] R. L. Wilmington, H. Ardekani, A. Rustagi, A. Bataller, A. F. Kemper, R. A. Younts, and K. Gundogdu, *Phys. Rev. B* **103**, 075416 (2021).
- [13] P. Cudazzo, I. V. Tokatly, and A. Rubio, *Phys. Rev. B* **84**, 085406 (2011).
- [14] T. C. Berkelbach, M. S. Hybertsen, and D. R. Reichman, *Phys. Rev. B* **88**, 045318 (2013).
- [15] J. Hubbard and R. E. Peierls, *Proc. R. Soc. London A* **240**, 539 (1957).



- [16] D. A. Kleinman, *Phys. Rev. B* **33**, 2540 (1986).
- [17] M. Combescot and P. Nozieres, *J. Phys. C* **5**, 2369 (1972).
- [18] F. A. Rasmussen and K. S. Thygesen, *J. Phys. Chem. C* **119**, 13169 (2015).
- [19] W. S. Yun, S. W. Han, S. C. Hong, I. G. Kim, and J. D. Lee, *Phys. Rev. B* **85**, 033305 (2012).
- [20] K. He, N. Kumar, L. Zhao, Z. Wang, K. F. Mak, H. Zhao, and J. Shan, *Phys. Rev. Lett.* **113**, 026803 (2014).
- [21] K. F. Mak, K. He, J. Shan, and T. F. Heinz, *Nat. Nanotechnol.* **7**, 494 (2012).
- [22] T. Peña, S. A. Chowdhury, A. Azizimanesh, A. Sewaket, H. Askari, and S. M. Wu, *2D Mater.* **8**, 045001 (2021).
- [23] See Supplemental Material at <http://link.aps.org/supplemental/10.1103/PhysRevB.106.045206> for information about the Wannier-Mott model used in the paper.
- [24] K. F. Mak, K. He, C. Lee, G. H. Lee, J. Hone, T. F. Heinz, and J. Shan, *Nat. Mater.* **12**, 207 (2013).
- [25] H. M. Hill, A. F. Rigosi, C. Roquelet, A. Chernikov, T. C. Berkelbach, D. R. Reichman, M. S. Hybertsen, L. E. Brus, and T. F. Heinz, *Nano Lett.* **15**, 2992 (2015).
- [26] G. Gupta, S. Kallatt, and K. Majumdar, *Phys. Rev. B* **96**, 081403 (2017).
- [27] S. Park, N. Mutz, T. Schultz, S. Blumstengel, A. Han, A. Aljarb, L.-J. Li, E. J. W. List-Kratochvil, P. Amsalem, and N. Koch, *2D Mater.* **5**, 025003 (2018).
- [28] T. Wang, Z. Li, Z. Lu, Y. Li, S. Miao, Z. Lian, Y. Meng, M. Blei, T. Taniguchi, K. Watanabe, S. Tongay, W. Yao, D. Smirnov, C. Zhang, and S.-F. Shi, *Phys. Rev. X* **10**, 021024 (2020).
- [29] N. Cortés, O. Ávalos-Ovando, L. Rosales, P. A. Orellana, and S. E. Ulloa, *Phys. Rev. Lett.* **122**, 086401 (2019).
- [30] H. Kim, G. H. Ahn, J. Cho, M. Amani, J. P. Mastandrea, C. K. Groschner, D.-H. Lien, Y. Zhao, J. W. Ager, M. C. Scott, D. C. Chrzan, and A. Javey, *Sci. Adv.* **5**, eaau4728 (2019).
- [31] H. Kim, D.-H. Lien, M. Amani, J. W. Ager, and A. Javey, *ACS Nano* **11**, 5179 (2017).
- [32] A. E. Almand-Hunter, H. Li, S. T. Cundiff, M. Mootz, M. Kira, and S. W. Koch, *Nature (London)* **506**, 471 (2014).
- [33] M. Kira and S. W. Koch, *Phys. Rev. A* **73**, 013813 (2006).